COANDA EFFECT ON THE FLOWS THROUGH EJECTORS AND CHANNELS

Alexandru DUMITRACHE[*], Florin FRUNZULICA[**], Tudor IONESCU[**]

[*]"Gheorghe Mihoc – Caius Iacob" Institute of Mathematical Statistics and Applied Mathematics, Bucharest, Romania (alex_dumitrache@yahoo.com)
[**]Politehnica University, Bucharest, Romania (ffrunzi@yahoo.com, tudor.ionescu2006@upb.ro)

DOI: 10.19062/2247-3173.2018.20.21

Abstract: *Coanda effect consists of the tendency of a jet to adhere to and to flow around nearby solid boundaries. This general class of phenomena, which may be observed in both liquid and gaseous jets, are known as the Coanda effect.*

In this paper, interest in the detailed behavior of an existing Coandă ejector model is taken, used in propulsion systems. The goal is to investigate the influence of various geometric parameters and pressure ratios on the Coandă ejector performance.

The application of the Coandă effect to the directional control of a jet is also presented. Deviation of the thrust force by direct flow can be achieved by using the Coanda effect to change the angle of the primary jet engine exhaust nozzle.

Since single jet flows or multi-jet flows are extensively applied in conjunction with the Coandă surface, as confined or free jet flows, in the last part of the paper, further insight into complexities involving issues such as the variety of flow structure and the related bifurcation and flow instabilities are provided.

Thus, the conditions and the limits within which one can benefit from the advantages of Coandă-type flows are determined.

Keywords: *Coandă effect, Coandă ejector, jet deflection, stationary bifurcation, CFD*

1. INTRODUCTION

The phenomenon to adhering of a fluid jet to a convex solid surface, known as the Coandă effect, has applications in aviation and many others in industry, in particular to obtain nozzles with high thrust augmentation and to increase the maximum lift coefficient of a wing.

In recent years, due to the development of computing techniques, many numerical experiments have been carried out which have led to a more thorough investigation of this phenomenon and to the optimization of configurations that use this phenomenon to increase their performance.

Sometimes the Coandă effect should be avoided, such as for an air-conditioned room, because the mixing of the injected air with the air of the room is not optimal.

To define the conditions and the limits to which it is advantageous to use the Coandă effect, studies and experiments are needed to determine its influence with respect to the geometrical and flow parameters.

The Coandă ejector is an axisymmetric device that uses the injected primary flow on the inner curved surface and entrains the secondary flow (Fig. 1).

The main purpose of the Coandă ejector is to provide a high ratio of the induced mass flow rate to the primary mass flow rate.

A high pressure tank provides a primary flow, which will follow the curved contour of the ejector after the sonic throat, due to Coandă effect. The expansion or compression waves are created depending on the pressure at the outlet section of the primary nozzle and, as a result, a turbulent mixing zone is developed. The effect of various factors, such as the pressure ratio, primary nozzle and ejector configurations on the system performance is evaluated based on the performance parameters. The mixing layer growth plays a major role in optimizing the performance of the Coanda ejector as it decides the ratio of secondary mass flow rate to primary mass flow rate and the mixing length.

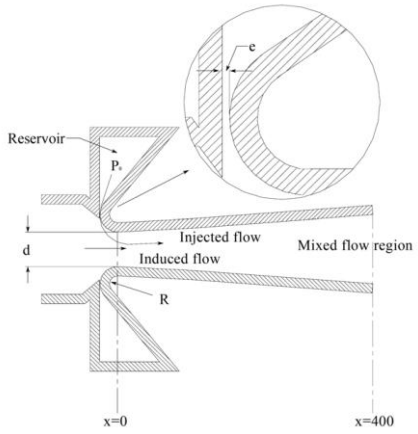

FIG 1. Schematic of the Coanda ejector

There are several works [1]-[5] investigating the mechanism through which the secondary flow is induced in the ejector. In this paper the authors study the various flow patterns inside the Coandă ejector and the effect of various design parameters on the mass flow rate of the induced flow numerically.

In the last part of the paper, further insight into complexities involving issues such as the variety of flow structure and the related bifurcation and flow instabilities are provided for the jet flowing to a wall by Coandă effect for several geometrical configurations.

Using the Ansys Fluent code, in this paper internal flows are analyzed, in order to determine the influence, advantages and limitations of the Coandă effect.

2. MATHEMATICAL MODEL

A. Dimensionless Forma of Fluid Transport Equation

Dimensionless quantities are universal, and independent of operating variables, such as fluid, geometric scale, operating pressure, etc. Therefore, all parameters in the research are converted to the dimensionless terms.

The fluid transport equations such as the mass (continuity), momentum, and energy conservation equations are presented in this section.

The mass conservation equation, or continuity equation, for the compressible flow is

$$\partial\rho/\partial t + \bar{\nabla}\cdot(\rho\bar{v}) = 0 \tag{1}$$

where: ρ = fluid density (kg/m^3), t = time (s), v = fluid velocity in a vector notation (m/s), $\bar{\nabla}$ = gradient operator.

The characteristic density and velocity are introduced to transform this equation to the dimensionless form. We define: ρ_c = characteristic (an inlet) density of the fluid (kg/m^3), U = characteristic (an inlet) velocity of the fluid (m/s), t_c = characteristic time (s), and L = characteristic length = an inlet diameter of ejector (m).

Then each term is converted to dimensionless form by multiplying and dividing each term by their characteristic parameters, and then rearranging the equation. Hence, the dimensionless form of this equation is presented in the following equation

$$\partial\tilde{\rho}/\partial\tilde{t} + \tilde{\nabla}\cdot(\tilde{\rho}\tilde{v}) = 0 \tag{2}$$

Momentum conservation for compressible flow in dimensional form is [6]:

$$\begin{aligned}\rho\frac{\partial}{\partial t}(\rho\bar{v}) + \overline{\nabla}\cdot(\rho\bar{v}\bar{v}) &= -\overline{\nabla}P_{dyn} + \mu\nabla^2\bar{v} + 2\overline{\nabla}\mu\cdot\overline{\nabla}\bar{v} \\ &+ \overline{\nabla}\mu\times(\overline{\nabla}\times\bar{v}) + \frac{1}{3}\mu\overline{\nabla}(\overline{\nabla}\cdot\bar{v}) - \frac{2}{3}(\overline{\nabla}\cdot\bar{v})\overline{\nabla}\mu\end{aligned} \tag{3}$$

where: D/Dt = material derivative, P_{dyn} = dynamic pressure (Pa), μ = fluid viscosity ($N\cdot m$), ∇^2 = Laplacian operator.

Since the geometrical configuration of the ejector is axisymmetric, the continuity equation will be used in axisymmetric coordinates

$$\frac{\partial\rho}{\partial t} + \frac{\partial}{\partial x}(\rho\bar{v}_x) + \frac{\partial}{\partial r}(\rho\bar{v}_r) + \frac{\rho\bar{v}_r}{r} = 0 \tag{4}$$

and the mass conservation equation in axisymmetric case is

$$\begin{aligned}\frac{\partial}{\partial t}(\rho\bar{v}_x) + \frac{1}{r}\frac{\partial}{\partial x}(r\rho\bar{v}_x\bar{v}_x) + \frac{1}{r}\frac{\partial}{\partial r}(r\rho\bar{v}_t\bar{v}_x) &= -\frac{\partial P}{\partial x} \\ &+ \frac{1}{r}\frac{\partial}{\partial x}\left[r\mu\left(2\frac{\partial\bar{v}_x}{\partial x} - \frac{2}{3}(\overline{\nabla}\cdot\bar{v})\right)\right] + \frac{1}{r}\frac{\partial}{\partial r}\left[r\mu\left(\frac{\partial\bar{v}_x}{\partial r} + \frac{\partial\bar{v}_r}{\partial x}\right)\right]\end{aligned} \tag{5}$$

B. The Energy Equation

In compressible fluid, the energy equation is used corporately with the transported equations to calculate fluid properties.

The governing energy equation is presented (Fluent, 2001):

$$\frac{\partial}{\partial t}(\rho E) + \overline{\nabla}\cdot\left[\bar{v}(\rho E + P)\right] = \overline{\nabla}\cdot\left[k_{eff}\overline{\nabla}T - \sum_j h_j\bar{J}_j + (\bar{\bar{\tau}}_{eff}\bar{v})\right] + S_h \tag{6}$$

where: E = internal energy (J), k_{eff} = effective conductivity (J/K), ∇T = total temperature difference (K), h_j = sensible enthalpy of species j (J), $\bar{J}_j$ = diffusion flux of species j, $\bar{\bar{\tau}}_{eff}$ = effective viscous dissipation ((Js)/m), and S_h = volumetric heat sources (J).

The equations can be spatially averaged to decrease computational cost, yet the averaging process yields a system with more unknowns than equations.

Hence, the unclosed system requires a model (e.g., turbulence, or subgrid scale) to make the problem well posed. Such models are used in RANS and LES approaches to CFD.

All the equations stated above are used to calculate fluid properties in CFD code, Fluent.

C. The Turbulence Modeling: SST Model Formulation

The basic idea behind the SST model is to retain the robust and accurate formulation of the Wilcox $k-\omega$ model in the near wall region, and to take advantage of the free stream independence of the $k-\varepsilon$ model in the outer part of the boundary layer.

In order to achieve this aim, the $k-\varepsilon$ model is transformed into a $k-\omega$ formulation by means a function that is one in the near wall region and zero away from the surface. The final form is

$$\frac{\partial}{\partial x_j}\left(u_j k\right)=\frac{\partial}{\partial x_j}\left[\left(\nu+\sigma_{k1}\nu_t\right)\frac{\partial k}{\partial x_j}\right]+P_k-Y_k \tag{7}$$

$$\frac{\partial}{\partial x_j}\left(u_j \omega\right)=\frac{\partial}{\partial x_j}\left[\left(\nu+\sigma_{\omega}\nu_t\right)\frac{\partial \omega}{\partial x_j}\right]+\gamma P_{\omega}-Y_{\omega}+$$
$$2\left(1-F_1\right)\sigma_{\omega 1}\frac{\nu_t}{k}\frac{\partial k}{\partial x_j}\frac{\partial \omega}{\partial x_j}$$

Model constants and implementation are presented in detail in [7], [8].

3. NUMERICAL MODEL

In the CFD study, the jet ejector model geometry matched the experimental apparatus. A commercial CFD code FLUENT with a preprocessor, GAMBIT is used to conduct the numerical analysis on the Coandă ejector. An axisymmetric Coandă ejector model is created with a structured and unstructured grid system with quadrilateral cells. The grid size was optimized to be small enough to ensure that the CFD flow results were virtually independent of size, but large enough to ensure the model run efficiently at an acceptable speed [9].

A non-uniform grid was selected because it provided the greatest control of the number of cells and their localized density. For optimal meshing, the grid density increased near the wall and in areas where flow gradients were steep.

This is accomplished by applying weighting factors to increase the grid density at these areas

The used mesh is divided in structured grid near the wall and unstructured grid otherwise. The y^+ values of the wall-next grid points were between 0.2 and 1, and the Δx^+ values were between 50 and 300.

The numerically results was obtained for a total pressure value of 5 bar, imposed at the reservoir inlet. The computational domain includes the adjacent regions of the ejector with the physical opening boundaries condition.

FLUENT is a density based finite volume computational fluid dynamics code which solves the three-dimensional or axisymmetric compressible Navier-Stokes equations in the desired domain. The flow is considered to be steady.

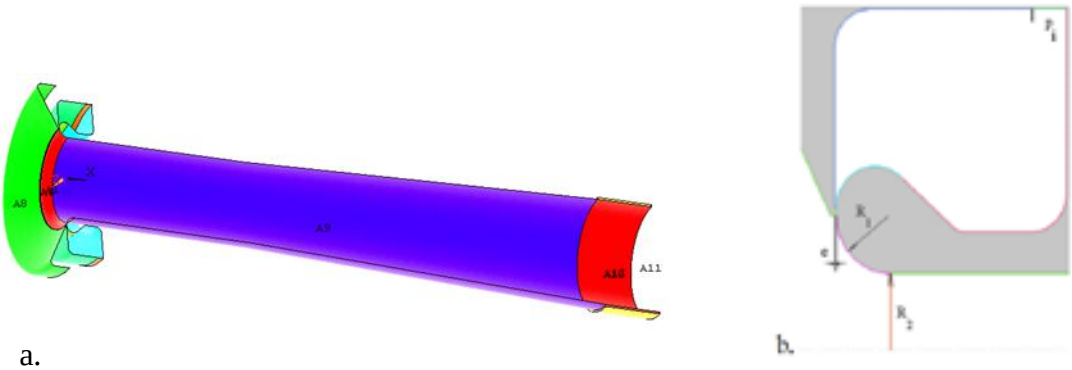

a.

FIG. 2. 3-D geometric Coandă ejector configuration (a.) and detail of the throat gap and Coandă surface – one primary jet (b.)

The following geometrical configurations are used (Fig. 2): $e_1 = 0.25$ mm, $e_2 = 0.40$ mm; $R_1 = 7.5$ mm and $R_2 = 37.5$ mm .

4. RESULTS AND DISCUSSIONS

The Mach number contours at the ejector throat are plotted in Fig. 3, and the pathlines patterns can be shown in Fig. 4, for this axisymmetric model of the standard Coandă ejector. From these figures it can be observed that the Mach contour show how the primary and induced flows mix in the divergent zone of the ejector, and that the induced flow does not follow the pathlines defined by the primary jet.

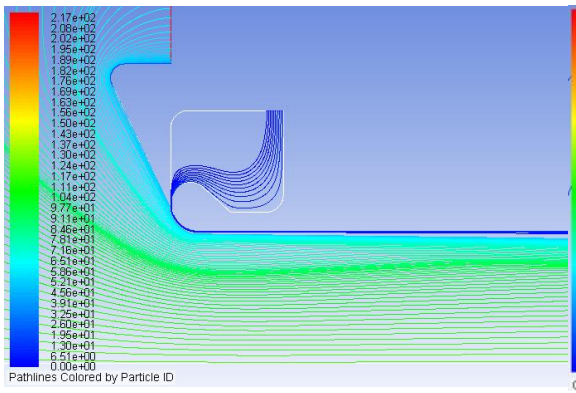

FIG. 3.. Pathlines pattern at the primary flow nozzle exit

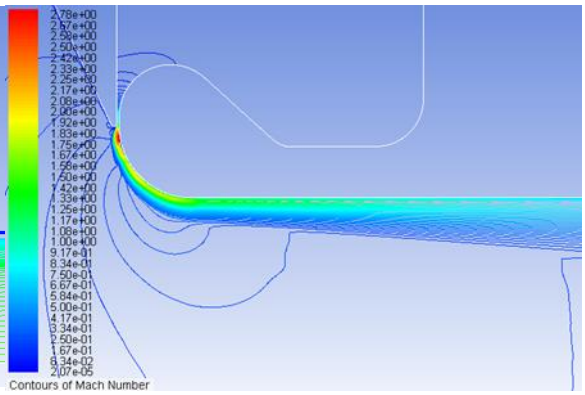

FIG. 4. Mach number contours at the ejector throat

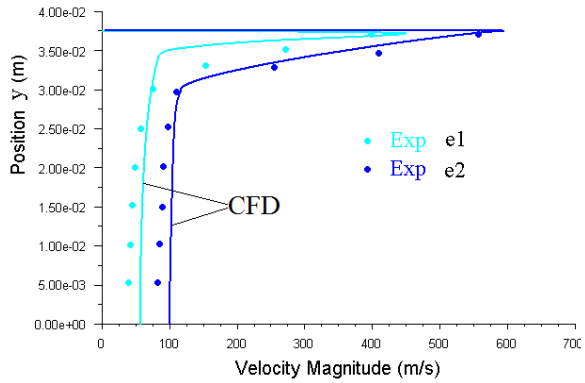

FIG. 5. Velocity profiles at x = 0.0 m

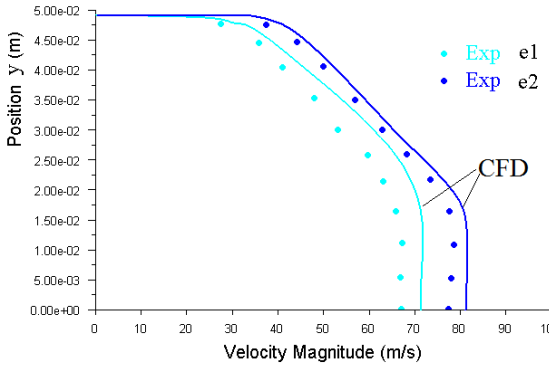

FIG. 6. Velocity profiles at x = 0.55 m

Figures 5-7 show the velocity magnitude or velocity profiles in different section of the ejector, for various primary nozzle gaps or other parameters (the Coandă surface radius, the inlet diameter).

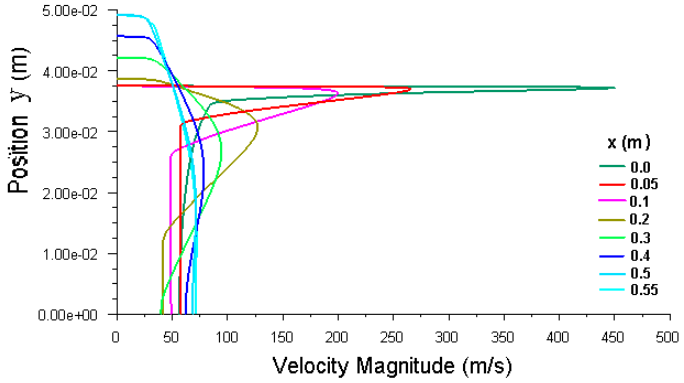

FIG. 7. Velocity magnitude in eight sections of the ejector (e_1=0.25)

The mixing characteristics can be estimated based on the velocity profile shape, which depends, in fact, on the measure of the nozzle throat gap. The flattened shape of the profile denotes an almost complete mixing ratio between the primary and the induced jets. If this is obtained in a section closer to the inlet, this yields a better ejector performance.

The ratio of the induced mass flow rate to the primary mass flow rate per stagnation pressure inside the reservoir can be considered as the Coandă ejector performance index.

All these numerical investigations, together with the experimental ones, demonstrate the importance of the geometry and the primary jet characteristics in optimizing the Coandă ejector.

5. COANDA EJECTOR WITH TWO PRIMARY JETS

In the sequel, the effect of a Coandă ejector with multiple primary jets is analyzed, using the same steady RANS equations. The geometry of the analyzed configuration is shown in Fig. 8 (a, b). The computation grid (hybrid) is constructed with approx. 277,765 cells and has 161,155 nodes. Near the solid boundaries, the first node is positioned at 1e-6 m to provide the numerical representation of the viscous sublayer ($y^+ \approx 1$), the cell growth rate being 1.05.

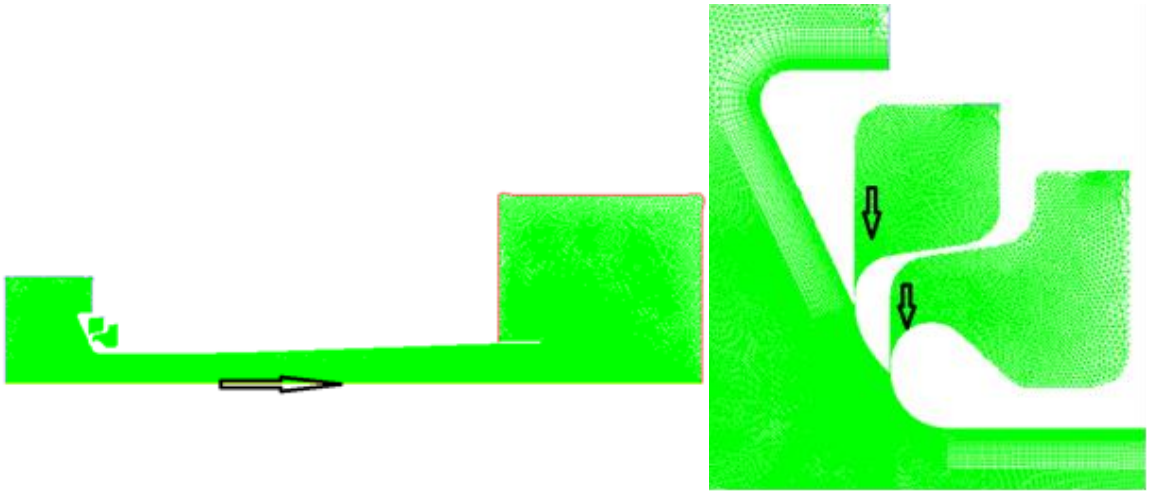

a) b)

FIG. 8. The computing grid used for simulations a.); details for primary jets b.)

Since the supply pressure of the primary nozzles is high, the jets are supersonic at the nozzle outlet, requiring a numerical density-based approach, the implicit scheme. To accelerate the convergence process, the first-order spatial meshing numerical scheme is chosen. Once the convergence of 10^{-3} has been reached for the primitive variables, the computation switches to the second order scheme for the equations describing the flow, the equations for the turbulent kinetic energy and the specific dissipation rate. The number of iterations needed to achieve convergence is of order 10^4.

The following cases have been simulated:

1 .a.,b. The first primary nozzle closed and the second supplied from a reservoir with a pressure of: 3 bar - (a) and 6 bar - (b);

2 . Both primary nozzles supplied from a reservoir with a 3 bar pressure.

Fig. 9 shows the streamlines through the Coandă ejector in the mentioned configurations. Note that the attachment of the jet (supersonic) on the convex surfaces

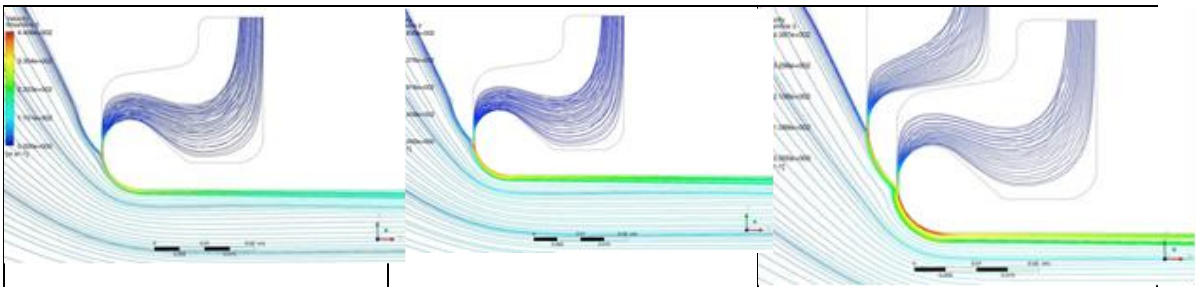

1.a 1.b 2.

FIG. 9. Streamlines for the three analyzed cases (detail around the primary nozzles – 1.a, 1.b and 2.)

and entrainment of the air in front of the ejector. Fig. 10 shows the pressure distribution in the vicinity of the primary nozzles, for all three cases. Due to the pressure difference between the reservoir(s) and the middle area of the ejector, the critical flow parameters are reached in the nozzles, the formed jet being supersonic.

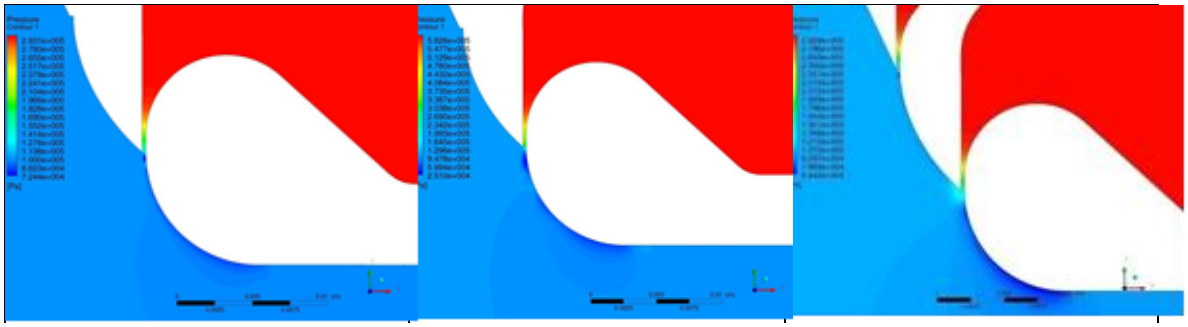

1.a 1.b 2.

FIG. 10. The pressure distribution around the primary nozzles for all three cases (1.a, 1.b and 2.)

Fig. 11 shows the velocity profiles in some typical sections (x_s = 0, 0.01, 0.025, 0.05, 0.075 m). The typical shape of the velocity profile for a jet in the presence of a surface is observed, as well as the effect of entrainment of the air through the ejector.

Table 1 shows the mass flow through the primary nozzles and through the inlet of the ejector.

Taking as reference case 1.a, note that in case 1.b the mass flow will increase with (0.64699-0.372522)/0.372522 x 100 % = 73.67 % and in the case of multiple ejector with (0.5776677-0.372522)/0.372522 x 100 % = 55.06 %. Although the supply pressure is doubled for the simple ejector it is observed that the entrained air mass-flow is not significantly higher than in a case of a multiple ejector supplied at moderate pressure.

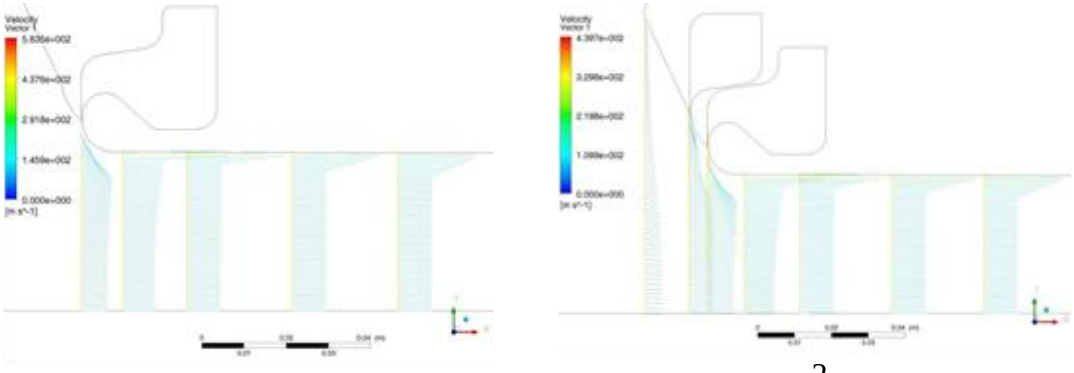

1.b. 2.

FIG. 11. Velocity profiles in some typical sections two cases (1.b., 2.)

Table 1. Air mass flow through the ejector for the three cases

Case	Primary nozzle 1 [kg/s]	Primary nozzle 2 [kg/s]	Ejector inlet [kg/s]	Total mass flow through ejector [kg/s]
1.a	-----	0.04596412	0.32655846	0.37252258
1.b	-----	0.09327204	0.55371882	0.64699086
2.	0.0549416	0.04590953	0.47582627	0.57667746

From a technical point of view, it seems reasonable to use a multi-jet ejector supplied at moderate pressure rather than a simple high pressure ejector.

Another advantage is that of mixing layer growth in the ejector flow, which has the effect of increasing the performance of the ejector.

A weak point of the multiple nozzle ejector is related to its size increasing, to introduce a second air reservoir and, implicitly, increase its mass.

6. THRUST AND JET VECTORING

Mechanical deflection of the thrust involves engine nozzle deflection and, thus, physically modify of the main flow direction [5,6], but this can used complicatelly devices and actuators. Alternative method to mechanical deflection can be done using a secondary jet to entrainment the main jet (Fig. 12). The component force of the thrust vector $T_0, F_{z,tv}$ produces a pitch moment, $M_{z,tv}$ around airplane's center of gravity, allowing the airplane to be controlled in flight. This force is adimensionalisated to obtain the thrust coefficient $C_z = F_{z,tv}/T_o$, where C_z depends on the angle of the thrust vector

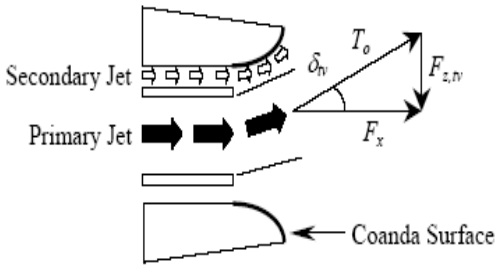

FIG. 12. The concept of thrust deviation

conform to equation $\delta_{tv} = \tan^{-1} C_z$. One must notice that deviation of the thrust force implies a change of the drag force. When $d_{tv} > 0$, the real force of the primar jet will be smaller then the resultant thrust force $F_x < T_o$.

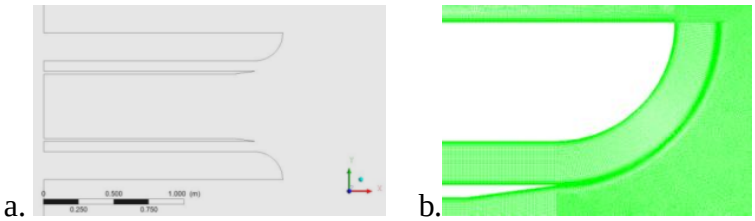

FIG. 13. The model used to highlight the change of the jet direction: a. the model geometry; b. detail of the computational grid.

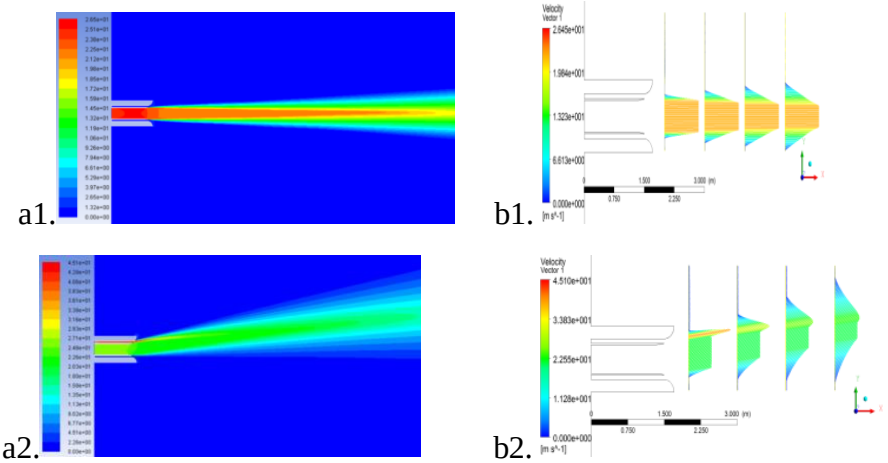

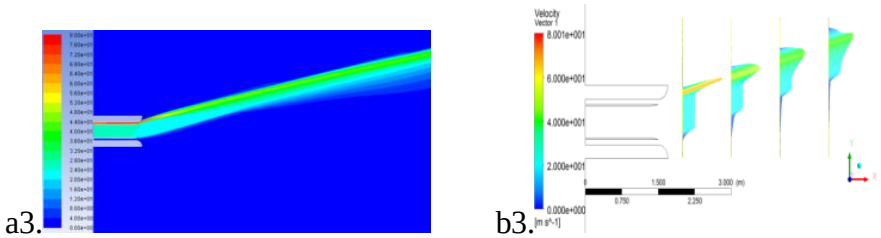

FIG. 14. The effect of secondary jet on the primary jet (Vj=25 m/s), the flow velocity field (a1-a3) and the velocity profiles (b1-b3) for 4 positions (2 m, 3 m, 4 m si 5 m).

The effect of the secondary flow on the main jet in the presence of a convex surface can be evidenced by numerical flow simulation on the configuration shown in Fig. 13. The main jet has a speed of 25 m/s, with a moderate turbulence degree. By varying the secondary jet velocity (considered only the upper jet in the presented geometric configuration), the results shown in Fig. 9 were obtained.

Figs. 14 a1-b1 correspond to a speed V_s = 0 m/s for the secondary jet, a2-b2 for V_s = 30 m/s, and a3-b3 for V_s = 70 m/s. From Fig. 9 it is observed that with the increase of the secondary jet velocity the deflection of the jet increases and the shape of the velocity profile in the main jet changes from a "full" velocity profile specific to the free jet to an asymmetric velocity profile with the maximum moved towards "the secondary jet". The deflection of the jet is "sustained" also by the shape of the exhaust surface (quarter circle). In Fig. 15 is shown the variation of the main jet angle deflection in relation to the secondary jet velocity.

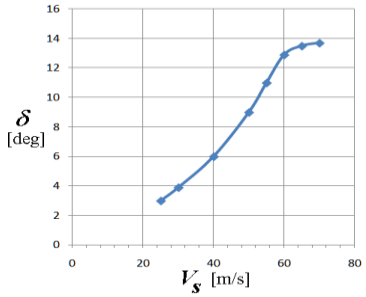

FIG. 15. The deflection of the main jet as function of the velocity of the secondary jet

If the secondary jet is accelerated over a Coandă surface, it will produce the local pressure drop and the appearance of the pressure gradient "perpendicular" to the main jet axis. This effect correlated with the friction effects leads to an increase in the fluid flow from the main jet to the secondary jet producing the change of the jet direction. Increasing the secondary jet velocity and the radius of curvature of the Coandă surface lead to a greater deflection of the main jet and obtaining the effect of the thrust vectorization. It is noted that for a secondary jet speed of over 60 m/s, the entrainment effect of the secondary jet decreases, the main jet being deflected very little or not at all.

7. STATIONARY BIFURCATION FLOW PHENOMENON INVESTIGATIONS

Qualitative changes occur in the structure of a flow, due to the Coandă effect, in some cases of two-dimensional channel flow configurations. In this paper two types of channel flows are numerically investigated, based on CFD approaches, in connection with the Coandă effect: the channel with or without sudden expansion inlet (y = 0 is a symmetry boundary, Fig. 16).

These qualitative changes are referred to as stationary bifurcations and in these cases they can be identified in the flow pattern as asymmetries that occur for certain values of the similarity parameter (Reynolds number, Rayleigh number), since, in general, the stationary Navier-Stokes boundary value problem is not uniquely solvable. These types of the instability phenomena or bifurcations may occur in fluid dynamics, already observed in early experiments [12], [13]. In [14] the pitchfork bifurcation flow in a symmetric 2D channel with contraction has been investigated.

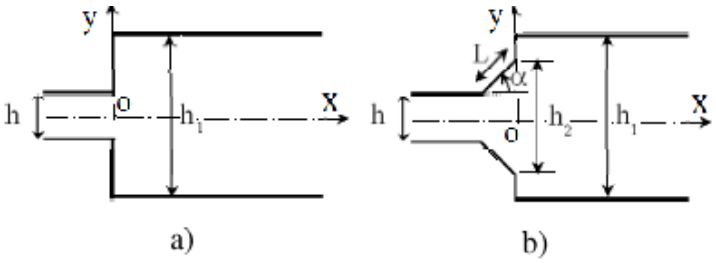

FIG.16. Geometry of the channel: a) sudden expansion; b) sudden expansion with divergent

A. The Physical and Numerical Formulation

The Navier-Stokes equations are governing the stationary, laminar, incompressible flow through the considered 2-D channels:

$$\begin{aligned} &\nabla \vec{V} = 0 \\ &\rho\left(\vec{V}\cdot\nabla\right)\vec{V} = -\nabla p + \mu\nabla^2\vec{V} \end{aligned} \tag{8}$$

$$u(y) = U_{\max}\left[1-\left(\frac{y}{y_{\max}}\right)^2\right] \tag{9}$$

where $y_{\max}$ is the channel width in the expansion zone (h or h_2). A no-slip boundary condition ($u = 0$) is imposed on the rigid walls of the channel and at the exit the boundary condition is applied, $\sigma \cdot n = 0$, where σ is the stress tensor and n is outward normal of the exit boundary.

The incompressible Navier-Stokes equations are solved using the SIMPLE (Semi-Implicit Method for Pressure Linked Equations) method introduced by Patankar [15]. The Reynolds number is based on velocity $U_{\max}$ and the height of the channel at the exit before the sudden expansion: $\mathrm{Re} = \rho U_{\max} h/\mu$, where ρ is the fluid density and μ is the dynamical viscosity.

B. Numerical Results and Discussions

Airflows characteristics have been numerically investigated through two channel configurations: sudden expansion, sudden expansion with divergent ($h_1 = h_2$).

For the sudden expansion configuration, the symmetry of the flow (Fig. 17) is noticed, but after the Reynolds number increases to a critical value of 228, the symmetry of the flow through the channel is lost, hence the flow becomes asymmetric (Fig. 18).

Regarding the wall shear-stress on the axial direction it is noted that it has different values for the upper and lower wall adjacent to the expansion zone and the recirculation area (where it has negative values).

There is a good correlation between the distribution of the wall shear stress and the length of the recirculation zone portion of the upper wall, respectively, lower.

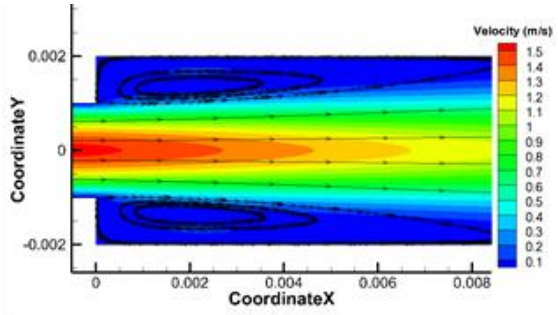

FIG. 17. The streamlines pattern and the velocity distribution before bifurcation, $\mathrm{Re} \approx 210$; ($h = 2$ mm, $h_1 = 4$ mm)

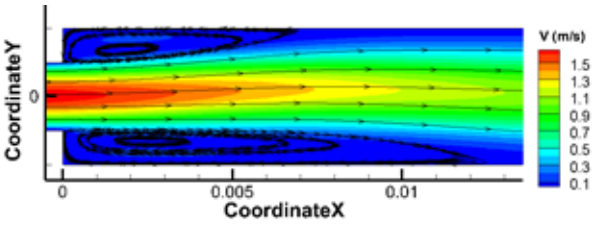

FIG. 18. The streamlines pattern and the velocity distribution after bifurcation, $\mathrm{Re} \approx 228$; ($h = 2$ mm, $h_1 = 4$ mm)

One of the recirculation zones is growing faster on one wall than the other, resulting in the attachment of the jet to this wall. The effect of this phenomenon occurring due to the impulse of a disturbance, is the deflection of the jet towards one of the walls. Hence the velocity is increasing along the wall, while the pressure is decreasing leading to the deflection of the jet. All these are actually the result of the Coandă effect.

In the second case, Fig. 19 shows the vertical velocity of the flow through the divergent channel with sudden expansion ($h_1 = h_2 = 8$ mm, $h = 2$ mm, $\alpha = 40$ deg) before the bifurcation (Re = 53), when the symmetry is observed. The grid has 92,000 quadrilateral cells with maximum resolution in the vicinity of the expansion zone, $2 \cdot 10^{-5}$ m.

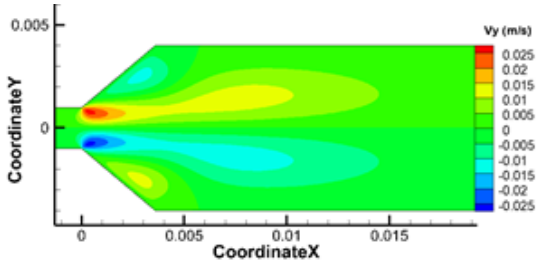

FIG. 19. The vertical velocity in the channel before bifurcation

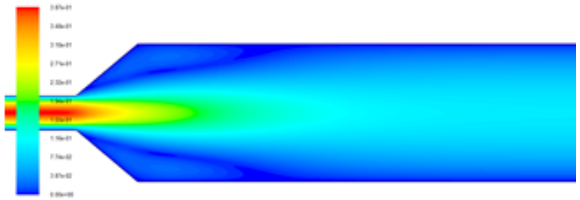

FIG. 20. Velocities spectrum through the channel with divergent before bifurcation, Re = 53 ($h_1 = h_2 = 8$ mm, $h = 2$ mm, $\alpha = 40$ deg)

Furthermore, Fig. 20 shows the absolute values of the velocities spectrum through the same channel under the same assumptions.

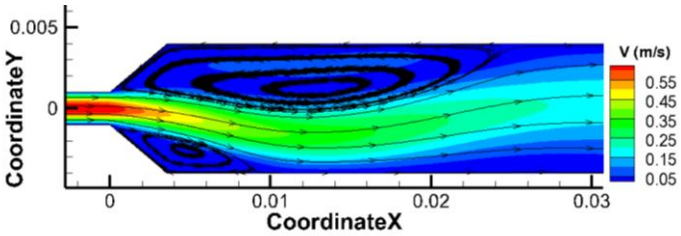

FIG. 21. The streamlines pattern and the velocity distribution after bifurcation, $\mathrm{Re} \approx 90$

If the Reynolds number goes over the value of 90, the symmetry of the flow vanishes as noted in Fig. 21.

These figures emphasize the asymmetries of the flow representing the bifurcations of the flow starting with the critical value of the Reynolds number. Note that these are stationary bifurcations.

Values of the critical Reynolds numbers (those from which bifurcations occur) decrease as the expansion ratio parameter increases ($k_e = h_1 / h$) or when the divergence angle (α) increases, as observed in numerical investigations.

For flows with Reynolds numbers larger than the critical values, the Hopf bifurcation phenomenon might occurs, which is periodic.

The critical values of the Reynolds number are corresponding to the values existing in the literature, yielded both numerically and experimentally [16]-[18].

CONCLUSIONS

By a computational study the effect of various geometric parameters on the performance of the Coandă ejector has been analyzed. The throat gap of the primary nozzle ('*e*') has a strong influence on the ratio of mass flow rates of the induced flow and the primary flow and a critical control over the mixing length as well. For reduced throat gaps, the mixing length decreased, and this possibly indicates the rapid mixing layer growth in the ejector.

The goal has been to investigate the influence of various geometric parameters and pressure ratios on the Coandă ejector performance. The effect of various factors, such as the pressure ratio, primary nozzle and ejector configurations on the system performance has been evaluated based on the performance parameters. The mixing layer growth plays a major role in optimizing the performance of the Coandă ejector as it decides the ratio of secondary mass flow rate to primary mass flow rate and the mixing length.

Also the effect of a Coandă ejector with multiple primary jets has been analyzed. From a technical point of view, it seems reasonable to use a multi-jet ejector supplied at moderate pressure rather than a simple high pressure ejector. Another advantage is that of mixing layer growth in the ejector flow, which has the effect of increasing the performance of the ejector.

The application of the Coandă effect to the directional control of a jet is presented. Deviation of the thrust force by direct flow can be achieved by using the Coanda effect to change the angle of the primary jet engine exhaust nozzle. This effect correlated with the friction effects leads to an increase in the fluid flow from the main jet to the secondary jet producing the change of the jet direction.

Because single jet flows or multi-jet flows are extensively applied in conjunction with the Coandă surface, as confined or free jet flows, in the last part of the paper we have provided further insight into complexities involving issues such as the variety of flow structure and the related bifurcation and flow instabilities. Qualitative changes occur in the structure of a flow, due to the Coandă effect, in some cases of two-dimensional channel flow configurations. These qualitative changes are referred to as stationary bifurcations and in these cases they can be identified in the flow pattern as asymmetries that occur for certain values of the similarity parameter (Reynolds number, Rayleigh number), since, in general, the stationary Navier-Stokes boundary value problem is not uniquely solvable.

For future work, further numerical and theoretical investigations will be done for more complex channel configurations at larger Reynolds numbers with the goal of determining the detailed physics of the flow through such channel. Furthermore, the advantages and the limitations of the use of the Coandă effect will be identified.

AKNOWLEDGMENT

This work has been supported by the grant of the Romanian National Authority for Research and Innovation, CNCS/CCDI-UEFISCDI, project number PN-III-P2-2.1-PED-2016-0376, within PNCDI III.

REFERENCES

[1] D. G. G. Smith, and A. R. Gilchrist, "The Compressible Coanda Wall Jet – An Experimental Study of Jet Structure and Breakaway" Intl. J. Heat and Fluid Flow, Vol.8, 1987, pp. 156-164.
[2] D. G. G Smith,. and P. Senior, "The Effect of Base Steps and Axisymmetry on Supersonic Jets over Coanda Surfaces", Intl. J. Heat and Fluid Flow, Vol.15, no.4, 1994, pp. 291-298.
[3] V. Guerriero, L. Baldas, and R. Caen, "Numerical Solutions of Compressible Flow Mixing in Coanda Ejectors", in CD-Rom Proc. The Eighth Symposium on Fluid Control, Measurement and Visualization, China (8FLUCOME), Q.-D. Wei and X.-G. Deng, Eds. Chengdu, China, 2005, pp. 343:1-7.
[4] A. Dumitrache, F., Frunzulica, O. Preotu, H. Dumitrescu, "Numerical analyis of turbulent flow in a Coanda ejector", Proc. Appl. Math. Mech., Vol. 11, pp. 647–648. doi: 10.1002/pamm.201110313.
[5] F. Frunzulica, A. Dumitrache, O. Preotu, "Control of two-dimensional turbulent wall jet on a Coanda surface", Proc. Appl. Math. Mech., Vol. 11, pp. 651–652. doi: 10.1002/pamm.201110315.
[6] J. Happel, H., Brenner, Low Reynolds Number hydro- dynamics, Englewood Cliffs, NJ: Prentice-Hall, 1965.
[7] F.R., Menter, "Eddy viscosity transport equations and their relation to the k- mode", ASME Journal of Fluids Engineering, vol. 119, 1997, pp. 876-884.
[8] R. Neuendorf, I. Wygnanski, "On a turbulent wall jet flowing over a circular cylinder", Journal of Fluid Mechanics, vol. 381, no. 1, 1999, pp. 1-25.
[9] S. B., Riffat, P. Everitt, P., "Experimental and CFD modeling of an ejector system for vehicle air conditioning", Journal of The Institute of Energy, vol. 491, 1999, pp. 41-47.
[10] Kim, H.D., Lee, J.H., Setoguchi, T., Matsuo, S.: Computational analysis of a variable ejector flow, Journal of Thermal Science, vol. 15, 2006, pp.140-144.
[11] T.H. Kim, A study on the characteristics of Coanda nozzle flow, Ph.D Thesis, Saga University, Japan, 2007.
[12] W. Cherdron, F. Durst, and J. Whitelaw, "Asymmetric flows and instabilities in symmetric channels with sudden expansion," Journal of Fluid Mechanics, vol. 84, pp. 13-31, 1978.
[13] I.J. Sobey, "Observation of waves during oscillating channel flow," Journal of Fluid Mechanics, vol. 151, pp. 395-426, 1985.
[14] A. Dumitrache, F. Frunzulica, and T. Ionescu, Mathematical modelling and numerical investigations on the Coanda effect, in: Nonlinearity, Bifurcation and Chaos - Theory and Applications, J. Awrejcewicz, and P. Hagedorn, Ed. InTech, 2012, pp. 101-132.
[15] S. Patankar, Numerical heat transfer and fluid flow, Hemisphere Publishing, pp. 125-134, 1980.
[16] C. Allery, J. M. Cadou, A. Hamdouni, and D. Razafindralandy, "Application of the Asymptotic Numerical Method to the Coanda effect study," Revue Européenne des Eléments Finis, Hermès, vol. 13, pp.57-77, 2004.
[17] D.M Hawken, P. Townsend, M.F. Webster, "Numerical simulation of viscous flows in channels with a step," Computers & Fluids, vol. 20, pp. 59-75, 1991.
[18] D. Drikakis, "Bifurcation in phenomena in incompressible sudden expansion flows," Phys. Fluids, vol. 9, pp. 76-87.